

Modelling and Simulation of a Wet Scrubber System

B.T.W. Mestemaker^{a,*}, E. Elmazi^b, L. van Biert^c, H.N. van den Heuvel^a, and K. Visser^c

^aRoyal IHC, Kinderdijk, The Netherlands

^bHeatmaster, Hendrik-Ido-Ambacht, The Netherlands

^cDelft University of Technology, Delft, The Netherlands

*btw.mestemaker@royalihc.com

Abstract

Shipping is a relatively clean transport method with low emissions per ton-mile compared with road transport. However, harmful emissions emitted in coastal areas are a concern, as these affect local air quality and health. To reduce sulphur oxide (SO_X) emissions, the International Maritime Organization (IMO) implemented a global sulphur cap of 0.5 wt% and the 0.1 wt% limit in emission control areas (ECAs). Ship owners can opt for either low sulphur fuels or wet scrubber systems. Wet scrubber systems are a reliable method for reducing SO_X emissions with capture rates of up to 98%. These systems may use seawater alkalinity or caustic soda (e.g. closed-loop systems) to neutralise the SO_X emissions. However, the dynamic loading of engines can cause large fluctuations in the exhaust flow conditions, and it is unknown how these affect the effectiveness of the scrubber. This study explores the impact of dynamic loads on the SO_X removal efficiency of closed-loop wet scrubbers. A dynamic model of a closed-loop wet scrubber utilising fresh water and caustic soda is developed and verified using publicly available data. The model applies the two-film theory to model the gas-liquid interface. Billet and Schultes liquid hold-up theory is used to model the liquid film thickness in the packed bed. Maintaining scrubber efficiency with large load fluctuations or high-frequency fluctuations requires an increased liquid flow. The scrubber control system used a set-point of 75% of the equivalent compliance limit to ensure compliance with the 0.1% ECA limit during load fluctuations. The model and results can be used to develop a more advanced control system for improved scrubber operation and integration with a selective catalytic reduction (SCR) system to demonstrate compliance with the IMO NO_X Tier III limit when using high-sulphur heavy fuel oil (HFO).

Keywords: Dynamics simulation; Modelling; Wet scrubber; System integration.

1 INTRODUCTION

The environment has taken up a crucial role in all decisions made during the 21st century. Many governments have implemented legislation to reduce greenhouse gas (GHG) emissions such as carbon dioxide (CO₂), methane (CH₄) and nitrous oxide (N₂O) emissions [1]. Shipping is currently a relatively clean form of transport with low emissions per ton-mile [2]. To ensure that the relative contribution of shipping does not increase in the future, the International Maritime Organization (IMO) has launched its initial GHG reduction strategy [3]. Additionally, the IMO has implemented measures such as the Energy Efficiency Design Index (EEDI), Energy Efficiency eXisting ship Index (EEXI), Ship Energy Efficiency Management Plan (SEEMP) and Carbon Intensity Indicator (CII) [4]–[6].

Harmful emissions such as nitrogen oxides (NO_X), sulphur oxides (SO_X) and particulate matter (PM) have become increasingly important due to their impact on human health, ecosystem acidification and eutrophication [7], [8]. The global

sulphur cap of 0.5 wt% implemented by the maritime industry on January 1st 2020 has significantly reduced the SO_X emissions. Shipping contributed about 5-8% of all global SO_X emissions before the implementation of the global sulphur cap in 2020 [9], [10].

There are several options to comply with the 0.5 wt% sulphur limit [11]. The solution may be found in the fuel choice such as a switch to very low sulphur fuel oil (VLSFO), distillate fuel, or liquefied natural gas (LNG). However, an abatement technology may also be applied to achieve the specified limit. The wet scrubber is the most widely applied SO_X emission reduction technology in the maritime sector and approximately 5000 ships are currently using such a system [12]. The three main wet scrubber types are as follows:

- An open-loop system with seawater used as the wash-water. The alkalinity of seawater is used to absorb and neutralise sulphur oxides.
- A closed-loop system in which fresh water and/or seawater is recycled. Caustic soda is used to absorb and neutralise the sulphur oxides.

- A hybrid system that uses seawater for the open-loop and seawater and/or fresh water with caustic soda for the closed-loop.

An open-loop system is implemented in approximately 81% of the cases, a hybrid system is implemented in about 17% and the remaining systems are closed-loop systems [12]. The majority of vessels equipped with scrubbers are cargo vessels crossing the ocean, sailing from port to port. Work vessels, such as dredging vessels have not yet been equipped with wet scrubber systems because of the limited available space on these vessels. Additionally, dredging vessels experience significant load changes from the dredge equipment, which may also affect the effectiveness of the scrubber.

The objective of this study is to investigate the impact of dynamic loads on the effectiveness of operating a closed-loop wet scrubber system with caustic soda. This is done to evaluate the potential of implementing such a system on vessels with highly transient loads, such as dredging vessels. The modelling methodology is discussed in Section 2. In Section 3, the simulations results are discussed, followed by the conclusions in Section 4, and future work in Section 5.

2 METHODS

The wet scrubber investigated in this study cleans the exhaust gas of an internal combustion engine (ICE) fuelled with high-sulphur heavy fuel oil (HFO). The scrubber uses scrubbing water (water mixed with caustic soda) for the absorption and conversion of the SO_X from the exhaust gas. The modelling of the scrubber process has been split between the gas phase, the liquid phase and the interface between both phases in which the SO_X absorption, water evaporation and heat transfer occur. This section discusses the modelling of the gas phase, the liquid phase and the interface between the gas and liquid phases.

2.1 Gas phase

The gas phase of the scrubber is modelled as a combination of resistance and volume elements as shown in Fig. 1. This method has been discussed in more detail by Schulten [13]. These elements are used to build complex systems in which gas flows. The venturi, packed bed, and demister are resistance elements, and the lower and upper volumes (volume below and above the packed bed) are volume elements. The venturi and demister sections are assumed to be simple resistance models, while

the packed bed is assumed to be the only location in which the SO_X absorption process occurs.

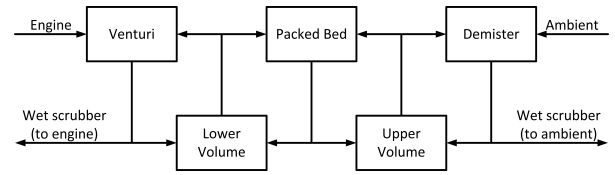


Figure 1: Schematic of wet scrubber model with resistance (upper row of blocks) and volume (lower row of blocks) elements

A resistance element as shown in Fig. 2 calculates the mass flow between the two volume elements as a function of the pressure drop. The element is modelled as an orifice, because there is no mass accumulation in it [13]. Equation 1 shows the mass flow calculation (ϕ^g) in the resistance element for an assumed incompressible flow [14] calculated using the effective area (A_{eff}) and resistance coefficient (ζ) of the orifice, pressure (p_{in}^g) and temperature (T_{in}^g) of the gas entering the resistance element, gas constant (R) and pressure ratio over the resistance element (π).

$$\phi^g = \frac{A_{eff}}{\sqrt{1 + \zeta}} \cdot \frac{p_{in}^g}{\sqrt{R \cdot T_{in}^g}} \cdot \sqrt{2} \cdot \sqrt{1 - \frac{1}{\pi}} \quad (1)$$

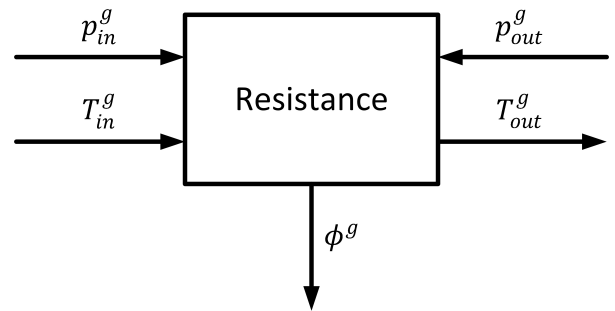


Figure 2: Resistance element (mass flow calculation)

A volume element as shown in Fig. 3 calculates the pressure in the element based on the mass flows entering and leaving the element, the temperature of the mass flow entering and the internal mass and energy balance [13]. The potential and kinetic energy terms are neglected in the volume element because these are small compared with the internal enthalpy [14].

The mass balance of the volume element is given by Eq. 2, where the mass change in the element ($\frac{dm_{cv}^g}{dt}$) is a function of the mass flow entering ($\phi_{cv,in}^g$) and leaving ($\phi_{cv,out}^g$) the element.

The temperature of the element is calculated using the energy balance of the control volume as shown in Eq. 3. The internal energy change ($\frac{d(m_{cv}^g \cdot u_{cv}^g)}{dt}$) in this equation is calculated using the mass flow ($\phi_{cv,in}^g$) and enthalpy ($h_{cv,in}^g$) of the flow entering the element, mass flow ($\phi_{cv,out}^g$) and enthalpy ($h_{cv,out}^g$) of the flow leaving the element, heat loss (q_{cv}^g) and work (w_{cv}^g) in the element. The pressure (p_{cv}^g) in the element was calculated using the ideal gas law, as shown in Eq. 4 with the gas constant (R), mass (m_{cv}^g) and temperature (T_{cv}^g) of the content of the element and the volume (V_{cv}^g) as parameters.

$$\frac{dm_{cv}^g}{dt} = \phi_{cv,in}^g - \phi_{cv,out}^g \quad (2)$$

$$\frac{d(m_{cv}^g \cdot u_{cv}^g)}{dt} = \phi_{cv,in}^g \cdot h_{cv,in}^g - \phi_{cv,out}^g \cdot h_{cv,out}^g + q_{cv}^g + w_{cv}^g \quad (3)$$

$$p_{cv}^g = \frac{m_{cv}^g \cdot R \cdot T_{cv}^g}{V_{cv}^g} \quad (4)$$

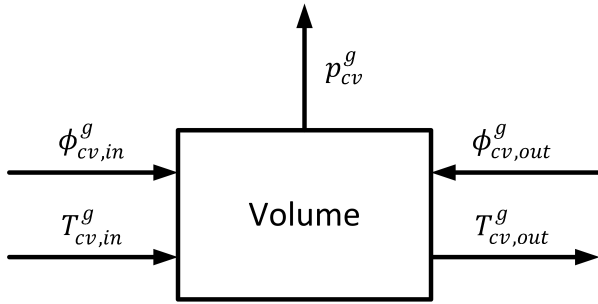


Figure 3: Volume element (pressure & temperature calculation)

The SO_X absorption, water evaporation and heat transfer between the gas and liquid phases occur in the packed bed section of the scrubber. The packed bed itself is modelled as a resistance element for the surrounding components. To improve the accuracy of the results, the packed bed was discretised using the same resistance and volume element approach, as shown in Fig. 4.

The removal of the SO_X , evaporation of water, and heat transfer occur in the internal volume elements of the packed bed. In these discretised elements, an interface between the gas and liquid phases is present, as shown in Fig. 5. The liquid (shown in blue) is fed to the top of the column and flows down owing to gravity, and the gas (represented in grey) is fed to the bottom and moves upward owing to pressure. Liquid and gas coexist in each discretised element. Absorption towers

are often filled with packing materials to improve the water distribution and create a large gas-liquid interface area [15].

Gas and liquid have contact in each section (for example, random section m in Fig. 5), and there is simultaneous mass and heat transfer between both phases. Both phases have their own control volumes for calculating their respective properties. There is a bidirectional flow between the control volumes for the mass flows of the absorbed sulphur dioxide (ϕ_{SO_2}) and the evaporated water ($\phi_{H_2O}^{evap}$) and the transfer of heat (q). Each gas control volume (m) receives its gas input from the previous discretised element ($m-1$) and each liquid control volume (m) receives its gas input from the previous discretised element ($m+1$). The interface between the gas and liquid phase is discussed in more detail in Section 2.3.

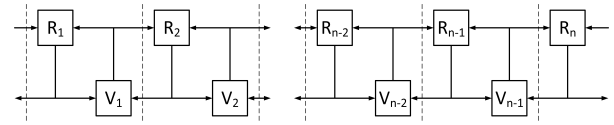


Figure 4: Packed bed gas phase discretisation to resistance and volume element

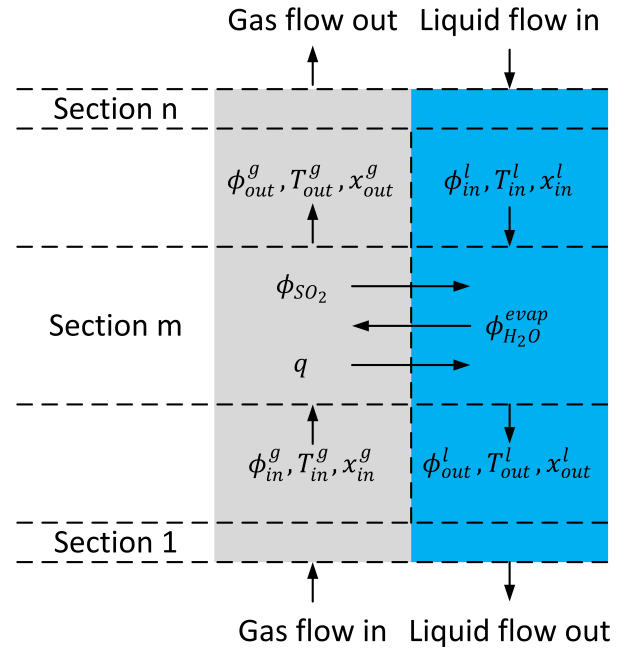


Figure 5: Packed bed presentation in n -sections with a detailed presentation of random section m

2.2 Liquid phase

The liquid water phase is modelled in the packed bed section of the scrubber to capture the adsorption process. Such an elaborate approach is omitted in the other sections because the majority of the SO_X

absorption takes place in the packed bed. The liquid phase of the other scrubber sections, as shown in Fig. 1, namely the venturi, lower and upper volumes, and demister, have not been modelled.

The liquid mass balance in the packed bed is governed by gravity alone. The slight pressure differences in the scrubber vessel that affect the gas phase are too small to affect water flow. Therefore, another approach must be applied to model the rate at which water flows through the packed bed. The mass balance of the liquid-phase ($\frac{dm_{pb}^l}{dt}$) is modelled according to Eq. 5 with the ingoing ($\phi_{pb,in}^l$) and outgoing flows ($\phi_{pb,out}^l$) and the water evaporating ($\phi_{H_2O}^{evap}$) as its parameters.

$$\frac{dm_{pb}^l}{dt} = \phi_{pb,in}^l - \phi_{pb,out}^l - \phi_{H_2O}^{evap} \quad (5)$$

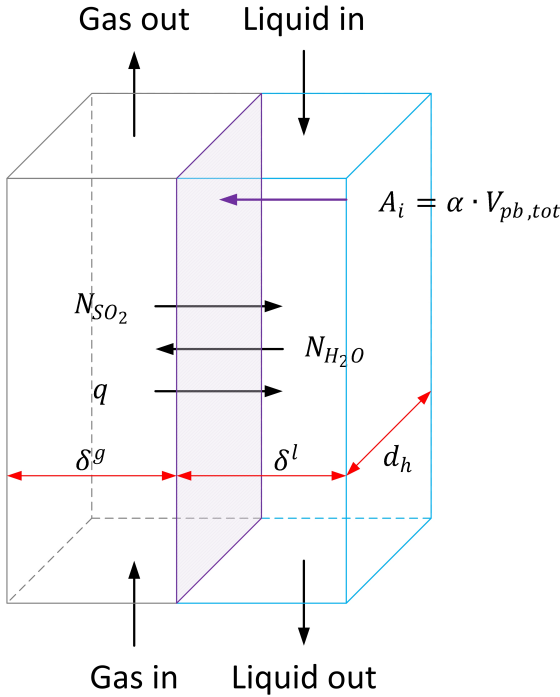


Figure 6: Schematic representation of the liquid gas interface in the model

The packed bed is irregular in shape and orientation, making it difficult to model. It is assumed that the packed bed may be modelled as a counterflow of liquid (downward) and gas (upward) in vertical flow channels (Fig. 6). The deviation between the real and modelled flows is the specific surface area (α) as shown in Eq. 6 to calculate the hydraulic diameter (d_h) of the vertical flow channels together with the void fraction (ϵ) [16].

$$d_h = 4 \cdot \frac{\epsilon}{\alpha} \quad (6)$$

The liquid film thickness (δ^l) in the packed bed is calculated using the ingoing ($\phi_{pb,in}^l$) and outgoing liquid flows ($\phi_{pb,out}^l$), water evaporating ($\phi_{H_2O}^{evap}$), liquid density (ρ^l), the specific surface area (α) and total volume of the packed bed ($V_{pb,tot}$) (Eq. 7).

$$\frac{d\delta^l}{dt} = \frac{\phi_{in}^l - \phi_{out}^l - \phi_{H_2O}^{evap}}{\rho^l \cdot \alpha \cdot V_{pb,tot}} \quad (7)$$

The liquid velocity in the packed bed (v_{cv}^l) is calculated using the empirical formula from Billet and Schultes for the liquid hold-up in packing materials [16]. Equation 8 calculates the velocity with the liquid hold-up (h^l), liquid density (ρ^l), cross-sectional area of the empty scrubber (A_{sc}), dynamic viscosity of the liquid (μ^l), specific surface area (α), hydraulic diameter (d_h) of the vertical flow channels, and liquid film thickness (δ^l).

$$v_{cv}^l = \frac{(h^l)^3 \cdot g \cdot \rho^l \cdot A_{sc}}{12 \cdot \mu^l \cdot \alpha^2 \cdot d_h \cdot \delta^l} \quad (8)$$

The changes in the liquid flow over the packed bed height are captured by discretisation of the packed bed model. The control volumes are assumed as ideally mixed elements. The mass flow leaving the control volume (ϕ_{cv}^l) is calculated using the liquid density (ρ^l), hydraulic diameter (d_h), liquid film thickness (δ^l) and liquid velocity in the packed bed (v_{cv}^l) (Eq. 9).

$$\phi_{cv}^l = \rho^l \cdot d_h \cdot \delta^l \cdot v_{cv}^l \quad (9)$$

2.3 Liquid-gas interface

The liquid-gas interface is where the heat and mass transfer between gas and liquid phases occurs. Sulphur oxides in the gas phase are absorbed by the liquid phase, where they react chemically with caustic soda (NaOH). Water evaporates from the liquid phase to the gas phase, while heat is transferred from the hot exhaust gases in the gas phase to the liquid phase.

The two-film theory introduced by Lewis and Whitman in 1924 is used to model the interface layers between the gas and liquid phases [17], [18]. The transport between both phases by molecular diffusion is limited by the mass-transfer resistance of the interface layers. The concentrations of the substances modelled are in equilibrium at the interface of both layers, but are not necessarily equal (Fig. 7). Figure 7 also shows a reaction plane for the chemical reaction between sulphur oxide and caustic soda. The chemical absorption of sulphur dioxide (SO₂) in the presence of hydroxide (OH⁻) may

be considered instantaneous and irreversible [19]–[21]. Therefore, the model introduced by Danckwerts [22] for instantaneous and irreversible reactions will be adopted. The concentration of sulphur dioxide decreases from the bulk gas value ($c_{SO_2,b}^g$) in the gas film towards the interface value of ($c_{SO_2,i}^g$). On the liquid side of the interface, the concentration is ($c_{SO_2,i}^l$) and it is constantly reduced. The reaction plane at distance (δ^r) in the liquid film is the location where it encounters the hydroxide concentration ($c_{OH^-}^l$) which has diffused through the liquid film at distance ($\delta^l - \delta^r$) from the bulk concentration ($c_{OH^-,b}^l$). Fick's law is used to model diffusion in the liquid film [23].

It is assumed that the reaction between the (SO_2) and the (OH^-) is completely performed in the reaction plane and that the (SO_2) does not reach the bulk of the liquid ($c_{SO_2,b}^l = 0$).

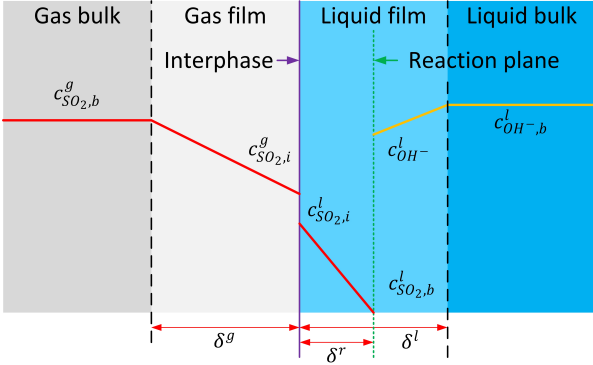


Figure 7: SO_2 and OH^- concentrations in the gas and liquid film and bulk

The mass transfer of sulphur dioxide (N_{SO_2}) is calculated using Eq. 10 and with the following parameters [24]–[26]: the mole fractions of sulphur dioxide ($y_{SO_2,b}^g$) in the gas and hydroxide ($y_{OH^-,b}^l$) in the liquid, the diffusion rate of sulphur dioxide ($D_{SO_2}^l$) and hydroxide ($D_{OH^-}^l$) in the liquid, Henry's constant for sulphur dioxide in the liquid ($H_{SO_2}^l$), the mass transfer coefficient for the gas (k_y^g) and the liquid (k_y^l), the gas pressure (p^g), the interface surface area (A_i) and the scrubber volume (V_{tot}).

Equation 11 is used to calculate the mass transfer of the water (N_{H_2O}) with the mass transfer coefficient for water (k_{y,H_2O}^g) in gas, the mole fractions of water in the gas ($y_{H_2O,b}^g$) and in liquid ($y_{H_2O,b}^l$), the saturated gas pressure (p_{sat}^l) and the gas pressure (p^g), the interface surface area (A_i) and the scrubber volume (V_{tot}) [26], [27].

$$N_{SO_2} = \frac{y_{SO_2,b}^g + \frac{H_{SO_2}^l}{p^g} \cdot \frac{D_{OH^-}^l \cdot y_{OH^-,b}^l}{2 \cdot D_{SO_2}^l}}{\frac{1}{k_y^g} + \frac{1}{k_y^l} \cdot \frac{H_{SO_2}^l}{p^g}} \cdot A_i \cdot V_{tot} \quad (10)$$

$$N_{H_2O} = k_{y,H_2O}^g \cdot (y_{H_2O,b}^g - y_{H_2O,b}^l \cdot \frac{p_{sat}^l}{p^g}) \cdot A_i \cdot V_{tot} \quad (11)$$

The heat transfer process from the (hot) gas to the (cold) liquid phase is illustrated in Fig. 8. The heat transfer follows from Eq. 12 with the following parameters [26]: the heat transfer coefficients for the gas (h_c^g) and the liquid (h_c^l) phases, the temperatures of the gas bulk (T_b^g), the interface area (T_i) and the bulk liquid (T_b^l), the specific surface area (α) and the total volume of the packed bed ($V_{pb,tot}$).

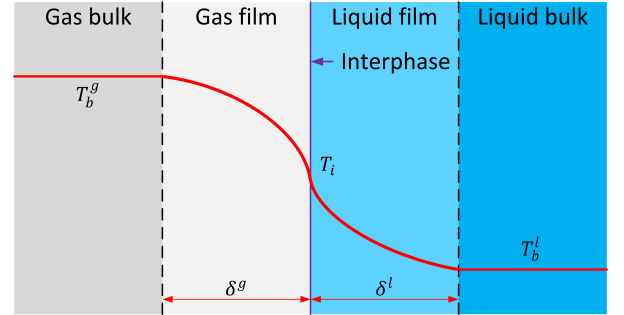


Figure 8: Temperature profile of the gas and liquid film and bulk

$$q = h_c^g \cdot \alpha \cdot V_{pb,tot} \cdot (T_b^g - T_i) = h_c^l \cdot \alpha \cdot V_{pb,tot} \cdot (T_i - T_b^l) \quad (12)$$

3 RESULTS

The simulations have been performed for a closed-loop wet scrubber suitable for a 6 cylinder 7.5 MW engine with the engine data provided in Table 1. The engine is assumed to operate at a constant excess air ratio of 2 and with an HFO with a fuel sulphur content of 3.5% [$\frac{m}{m}$].

The scrubber vessel has a diameter of 2.8 m and a height of 7.5 m of which it is assumed that the packed bed uses a height of 2.0 m. The packed bed in this study consists of a dumped packing of ceramic Hiflow rings with a diameter of 50 mm, resulting in 5120 rings per m^3 with a specific surface area (α) of $89.7 \frac{m^2}{m^3}$ and a void fraction (ϵ) of 0.809 $\frac{m^3}{m^3}$. The liquid flow has a hydroxide mass fraction (x_{OH^-}) of 0.000145 $\frac{kg}{kg}$.

Table 1: Engine data used for the simulations.

Load[%]	$\phi_{gas} [\frac{kg}{s}]$	Temperature[K]
25	5.08	573
50	8.91	538
75	10.9	565
100	13.0	611

The packed bed has been discretised to improve the accuracy of the model. A higher discretisation produces more accurate results, but also has longer simulation times. Figure 9 shows the effect of the discretisation on the liquid flow required to achieve the SO₂ removal efficiency. The scrubber must ensure compliance to the upper limit of 0.1% $\frac{m}{m}$ limit when operating in a Sulphur oxide Emission Control Area (SECA). The 0.1% $\frac{m}{m}$ limit is equivalent to $4.3 \frac{ppmv_{SO_2}}{y_{CO_2}}$ [28].

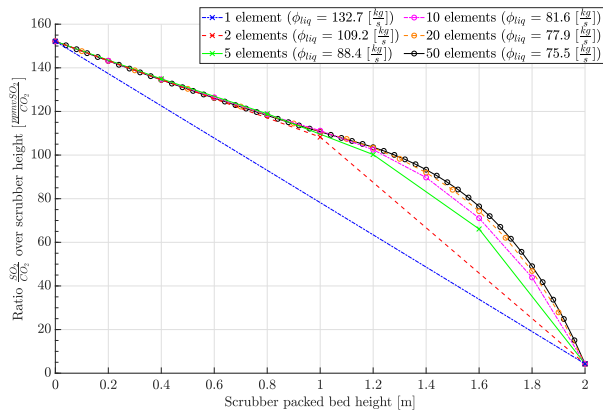


Figure 9: Liquid flow required to achieve the $4.3 \frac{ppmv_{SO_2}}{y_{CO_2}}$ limit for different packed bed discretisation sizes

The simulations in the remainder of this study will be performed with a discretisation of 10 steps as the results for 1,2 and 5 deviate significantly from those of 10, 20 and 50 steps. The liquid flow required to achieve the limit with 10 discretisation steps is $81.6 \frac{kg}{s}$, this is less than 5% higher than the $77.9 \frac{kg}{s}$ for 20 discretisation steps and 8% higher than the $75.5 \frac{kg}{s}$ for 50 discretisation steps while having a more acceptable calculation time.

Figures 10 and 11 show the longitudinal gas and liquid temperatures in the packed bed of the scrubber for each engine load point and the liquid flow required to achieve the $4.3 \frac{ppmv_{SO_2}}{y_{CO_2}}$ limit. The exhaust gas enters at a packed bed height of 0 m and exits at 2 m with a temperature of about 300 K. This is about 5 K above the liquid temperature of 295 K for all gas mass flows. The liquid flow enters the packed bed at 2 meters with a temperature of 295 K

and a flow of $81.6 \frac{kg}{s}$ and exits at the bottom (0m) with a temperature increases of around 11-16K.

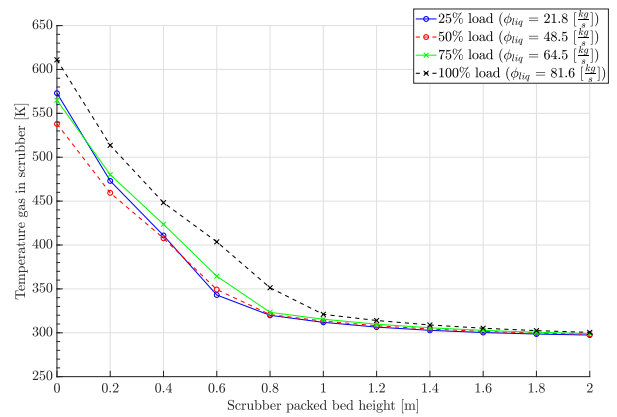


Figure 10: Longitudinal gas temperature for each engine load point

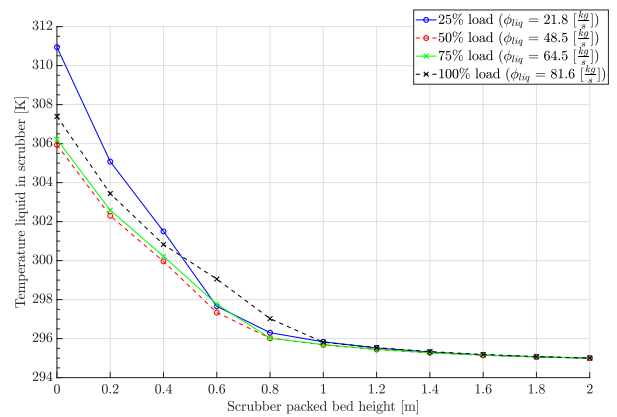


Figure 11: Longitudinal liquid temperature for each engine load point

The impact of transient engine loading on the scrubber performance is tested using the data given in Table 1 by cycling through these load points. The scrubber model is dynamic, but on the engine side a quasi-static approach is used which neglects the impact of among others the turbocharger behaviour on the exhaust gas mass flow, temperature and composition. The pump-pipe dynamics have been simplified with a rate limiter to include the effect of accelerating and decelerating the scrubber liquid flow. The liquid flow of the scrubber is controlled with a Proportional Integral (PI)-controller with a set-point of $3.225 (= 4.3 \cdot 75\%) \frac{ppmv_{SO_2}}{y_{CO_2}}$ to ensure compliance to the 0.1 wt% SECA limit during the load fluctuations. This set-point requires a liquid flow of $82.5 \frac{kg}{s}$ at 100% maximum continuous rating (MCR).

Several vessel types, such as dredging vessels, experience load fluctuations owing to the nature of their operation [29]. This may impact the effective

SO_X removal of the scrubber, and therefore, the impact of two fluctuation sizes will be tested, namely 25%-100% maximum continuous rating (MCR) and 75%-100% MCR.

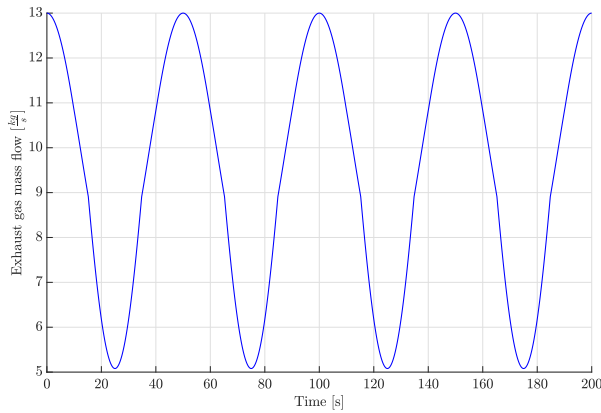


Figure 12: Exhaust gas mass entering the scrubber (100% – 25% – 100%)

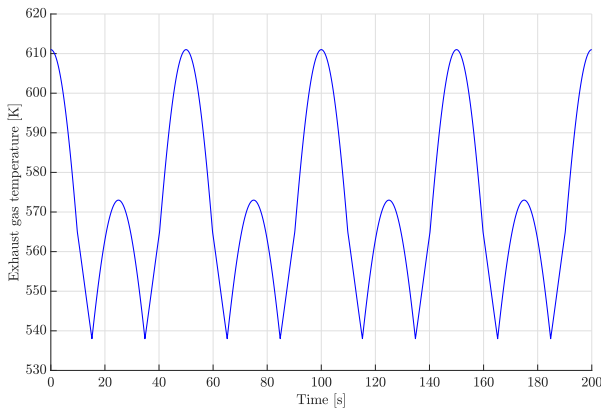


Figure 13: Exhaust gas temperature entering the scrubber (100% – 25% – 100%)

Figures 12 and 13 show the exhaust gas mass flow and temperature entering the scrubber for fluctuations between 25% and 100% MCR with a period of 50 s. The liquid flow during the dynamics exceeds the flow required to achieve the set-point of $3.225 \frac{ppmv_{SO_2}}{y_{CO_2}}$ ($82.5 \frac{kg}{s}$) at nominal load with about 7.0% ($88.3 \frac{kg}{s}$) for the simulation with evaporation and with about 2.7% ($84.7 \frac{kg}{s}$) if evaporation is not included as shown in Fig. 14. The scrubber remains within the compliance limit, as shown in Fig. 15.

The inclusion of evaporation in the simulation model appears to result in an instability of the liquid flow and the $\frac{ppmv_{SO_2}}{y_{CO_2}}$ ratio during this simulation. However, the validity of this instability is uncertain because the model has not been validated.

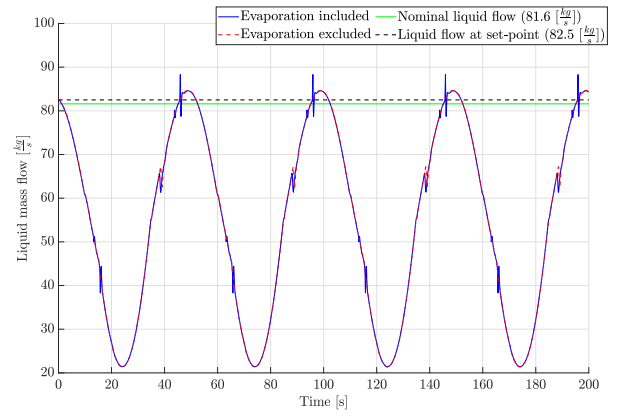


Figure 14: Scrubber liquid flow including and excluding the evaporation influence (100% – 25% – 100%)

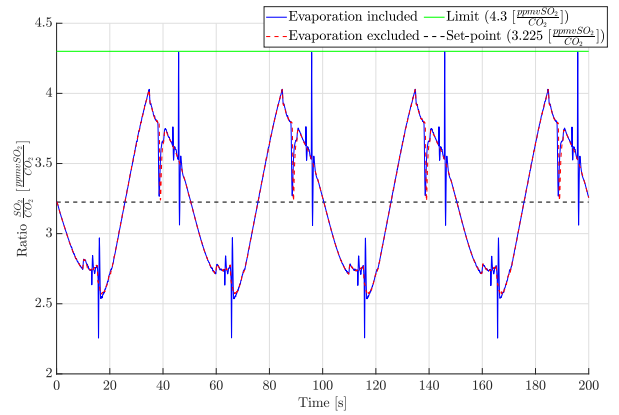


Figure 15: Fraction of $\frac{ppmv_{SO_2}}{y_{CO_2}}$ leaving the scrubber including and excluding the evaporation influence (100% – 25% – 100%)

The 75%-100% MCR simulations have been performed with a period of 50 and of 10 s to observe the impact of a faster load change. The simulations include the effect of water evaporation. Figure 16 shows that the liquid flow exceeds the nominal value for the 50 s period by about 0.1% ($82.6 \frac{kg}{s}$) and by about 3.6% ($85.5 \frac{kg}{s}$) for the 10 s period.

Figure 17 shows that the ratio of $\frac{ppmv_{SO_2}}{y_{CO_2}}$ is more stable for the 50 second period than for the 10 second period. This means that for applications in which fast load changes occur a larger margin to the SECA limit is required to ensure compliance, whereas for applications with slower changes, a smaller margin will suffice. The application of a more advanced control system may result in a more stable $\frac{ppmv_{SO_2}}{y_{CO_2}}$ ratio, but it will not compensate for the slow response of the pump-pipe system, which must be overcome for the load changes.

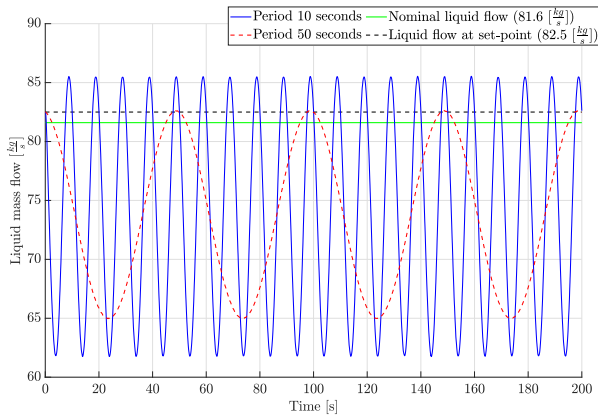


Figure 16: Scrubber liquid flow (100% – 75% – 100%)

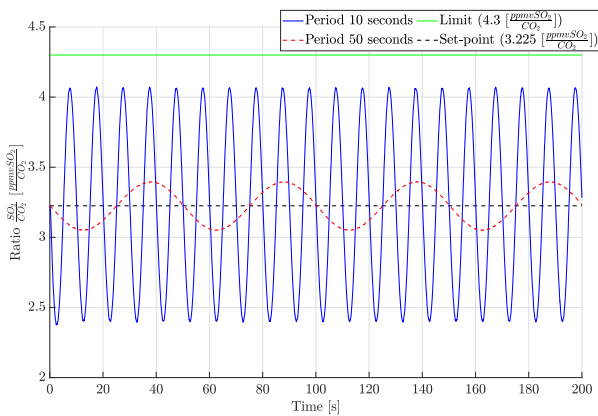


Figure 17: Fraction of $\frac{ppmv_{SO_2}}{y_{CO_2}}$ leaving the scrubber (100% – 75% – 100%)

4 CONCLUSIONS

Wet scrubbers are capable of effectively removing sulphur oxide emissions from the exhaust gas of vessels with dynamically loaded engines. A feedback control system with a sufficient margin in the set-point is sufficient to maintain the SO_x emissions well within the dictated limit.

The inclusion of evaporation in the model results in instability of the $\frac{ppmv_{SO_2}}{y_{CO_2}}$ ratio in the model owing to the evaporation of liquid in the packed bed and condensation in the demister. This may result in a scrubber that momentarily exceeds the dictated limit.

discretisation of the packed bed model improves the accuracy of the SO₂ removal efficiency calculation. This increase in accuracy comes at the cost of additional calculation time. The calculation results converge from the discretisation of 10 steps, whereas for this number of discretisation steps, the calculation time is still acceptable.

5 FUTURE WORKS

The model and its results should be validated to examine the accuracy of the SO_x removal efficiency and the impact of evaporation on the scrubber performance. The impact of evaporation may have to be ignored in future research if the behaviour shown in the 25%-100% MCR simulations is an effect of the simulation and modelling approach and does not occur in actual systems.

A more advanced control system may be considered based on a feed-forward signal from the engine (e.g. engine load and fuel rack position), in combination with the feedback signal from the exhaust gas composition. This solution may result in a better controlled liquid flow without overshooting the nominal value. Additionally, this could result in the system operating with less margin in the liquid flow, which reduces the power consumption of the scrubber.

The scrubber model may also be integrated with an engine model and/or run measurement data to determine the impact of actual load fluctuations on the operation and sulphur oxide removal efficiency of the scrubber. This shows the impact of a combined change in the exhaust gas mass flow and mass fractions of sulphur oxide in the exhaust gas. In addition, integration with a selective catalytic reduction (SCR) system may demonstrate compliance with the IMO NO_x Tier III limit when using high-sulphur heavy fuel oil (HFO).

The packed bed modelling method may be changed from a resistance-volume element system to a plug flow model. This allows for more discretisation of the packed bed and a higher accuracy of the simulation results without a significant impact on the calculation time.

ACKNOWLEDGEMENTS

This research is based on the work performed within the MSc thesis work of Enri Elmazi named: “Closed Loop Wet Scrubber System for Maritime Application: Dynamic Modelling and System Integration” at Delft University of Technology.

REFERENCES

- [1] S. Gössling, C. Meyer-Habighorst, and A. Humpe, “A global review of marine air pollution policies, their scope and effectiveness,” *Ocean & Coastal Management*, vol. 212, p. 105 824, 2021, ISSN: 0964-5691.

- [2] IMO, *Second imo ghg study 2009*, <https://wwwcdn.imo.org/localresources/en/OurWork/Environment/Documents/SecondIMOGHGStudy2009.pdf>, 2009.
- [3] IMO, *Initial imo strategy on reduction of ghg emissions from ships, resolution mepc.304(72)*, [https://wwwcdn.imo.org/localresources/en/KnowledgeCentre/IndexofIMOResolutions/MEPCDocuments/MEPC.304\(72\).pdf](https://wwwcdn.imo.org/localresources/en/KnowledgeCentre/IndexofIMOResolutions/MEPCDocuments/MEPC.304(72).pdf), 2018.
- [4] IMO, *Amendments to the annex of the protocol of 1997 to amend the international convention for the prevention of pollution from ships, 1973, as modified by the protocol of 1978 relating thereto, amendments to marpol annex vi, procedures for sampling and verification of the sulphur content of fuel oil and the energy efficiency design index (eedi), resolution mepc.324(75)*, [https://wwwcdn.imo.org/localresources/en/KnowledgeCentre/IndexofIMOResolutions/MEPCDocuments/MEPC.324\(75\).pdf](https://wwwcdn.imo.org/localresources/en/KnowledgeCentre/IndexofIMOResolutions/MEPCDocuments/MEPC.324(75).pdf), 2020.
- [5] IMO, *Report of the marine environment protection committee on its seventy-fifth session*, [https://www.mpa.gov.sg/docs/mpalibraries/mpa-documents-files/shipping-division/mepc-reports/mepc-75-18---report-of-the-marine-environment-protection-committeeon-its-seventy-fifth-session-\(secretariat\).pdf](https://www.mpa.gov.sg/docs/mpalibraries/mpa-documents-files/shipping-division/mepc-reports/mepc-75-18---report-of-the-marine-environment-protection-committeeon-its-seventy-fifth-session-(secretariat).pdf), 2020.
- [6] IMO, *Report of the marine environment protection committee on its seventy-sixth session*, [https://www.mpa.gov.sg/docs/mpalibraries/mpa-documents-files/shipping-division/mepc-reports/mepc-76-15---report-of-the-marine-environment-protection-committee-on-its-seventy-sixth-session-\(secretariat\).pdf](https://www.mpa.gov.sg/docs/mpalibraries/mpa-documents-files/shipping-division/mepc-reports/mepc-76-15---report-of-the-marine-environment-protection-committee-on-its-seventy-sixth-session-(secretariat).pdf), 2021.
- [7] IMO, *Amendments to the annex of the protocol of 1997 to amend the international convention for the prevention of pollution from ships, 1973, as modified by the protocol of 1978 relating thereto (revised marpol annex vi), resolution mepc.176(58)*, [https://wwwcdn.imo.org/localresources/en/OurWork/Environment/Documents/176\(58\).pdf](https://wwwcdn.imo.org/localresources/en/OurWork/Environment/Documents/176(58).pdf), 2008.
- [8] E. Ytreberg, S. Åström, and E. Fridell, “Valuating environmental impacts from ship emissions – the marine perspective,” *Journal of Environmental Management*, vol. 282, p. 111 958, 2021, ISSN: 0301-4797.
- [9] K. Cullinane and S. Cullinane, “Chapter 3 - policy on reducing shipping emissions: Implications for “green ports”,” in *Green Ports*, R. Bergqvist and J. Monios, Eds., Elsevier, 2019, pp. 35–62, ISBN: 978-0-12-814054-3. [Online]. Available: <https://www.sciencedirect.com/science/article/pii/B9780128140543000037>.
- [10] L. v. Biert, “Solid oxide fuel cells for ships: System integration concepts with reforming and thermal cycles,” Ph.D. dissertation, Delft University of Technology, 2020, ISBN: 9789463662482.
- [11] M. Tadros, M. Ventura, and C. Guedes Soares, “Review of current regulations, available technologies, and future trends in the green shipping industry,” *Ocean Engineering*, vol. 280, p. 114 670, 2023, ISSN: 0029-8018.
- [12] DNV. “Alternative fuels insight, scrubbers.” (2023), [Online]. Available: <https://afi.dnvg1.com/statistics/DDF10E2B-B6E9-41D6-BE2F-C12BB5660107>.
- [13] P. Schulten, “The interaction between diesel engines, ship and propellers during manouevring,” Ph.D. dissertation, Delft University of Technology, 2005, ISBN: 9789040725791.
- [14] D. Stapersma, “Diesel engines, a fundamental approach to performance analysis, turbocharging, combustion, emissions and heat transfer, part i, performance analysis and turbocharging, volume 2, turbocharging,” Royal Netherlands Naval College, Tech. Rep., 2010.
- [15] V. Bontozglou, *Introduction to Physical Processes, Theoretical Background and Basic Applications (translated from Greek)*, Greek. Kallipos Publications, 2015, ISBN: 9786188212473.
- [16] R. Billet and M. Schultes, “Prediction of mass transfer columns with dumped and arranged packings: Updated summary of the calculation method of billet and schultes,” *Chemical Engineering Research and Design*, vol. 77, no. 6, pp. 498–504, 1999, ISSN: 0263-8762.
- [17] W. Lewis and W. Whitman, “Principles of gas absorption.”, *Industrial & Engineering Chemistry*, vol. 16, pp. 1215–1220, 1924.
- [18] R. A. Zaveri, R. C. Easter, J. E. Shilling, and J. H. Seinfeld, “Modeling kinetic partitioning of secondary organic aerosol and size distribution dynamics: Representing effects of volatility, phase state, and particle-phase reaction,” *Atmospheric Chemistry and Physics*, vol. 14, no. 10, pp. 5153–5181, 2014.
- [19] J. Dean, *Lange’s handbook of chemistry*. McGraw-Hill, Inc., 1998, 1424 pp., ISBN: 9780070163843.
- [20] G. Vázquez, G. Antorrena, F. Chenlo, and F. Paleo, “Absorption of so2 by aqueous naoh solutions in the presence of a surfactant,” *Chemical Engineering & Technology*, vol. 11, no. 1, pp. 156–162, 1988.
- [21] D. Flagiello, F. Di Natale, A. Lancia, *et al.*, “Experimental and modelling approach to the design of chemical absorption columns with fast gas-liquid reaction: A case-study on flue-gas desulfurization with h2o2 oxidative solutions,” *Chemical Engineering Research and Design*, vol. 194, pp. 425–438, 2023, ISSN: 0263-8762.
- [22] P. Danckwerts, *Gas-liquid reactions*. McGraw-Hill Book Company, 1970, ISBN: 9780070152878.

- [23] W. Chen, Y. Chen, and C. Hung, "A simplified model of predicting SO₂ absorption by single atmospheric raindrops with chemical dissociation and internal circulation," *Aerosol and Air Quality Research*, vol. 11, no. 7, pp. 860–872, 2011.
- [24] M. Schultes, "Absorption of sulphur dioxide with sodium hydroxide solution in packed columns," *Chemical Engineering & Technology*, vol. 21, no. 2, pp. 201–209, 1998.
- [25] M. Schlager, M. Baumfrisch, G. Haushofer, V. Wolf-Zöllner, and M. Lehner, "Mass transfer model of packed seawater scrubbers for marine exhaust gas cleaning," *Chemical Engineering Research and Design*, vol. 192, pp. 128–140, 2023, ISSN: 0263-8762.
- [26] R. Bird, W. Stewart, E. Lightfoot, and D. Klingenberg, *Introductory Transport Phenomena*. Wiley, 2015, ISBN: 9781118953716.
- [27] W. Johansson, J. Li, and L. Lin, "Module-based simulation model for prediction of convective and condensational heat recovery in a centrifugal wet scrubber," *Applied Thermal Engineering*, vol. 219, p. 119 454, 2023, ISSN: 1359-4311.
- [28] IMO, *2021 guidelines for exhaust gas cleaning systems, resolution mepc.340(77)*, https://puc.overheid.nl/nsi/doc/PUC_701345_14/1/, 2021.
- [29] B. Mestemaker, M. Goncalves Castro, H. van den Heuvel, and K. Visser, "Dynamic simulation of a vessel drive system with dual fuel engines and energy storage," *Energy*, vol. 194, p. 116 792, 2020, ISSN: 0360-5442.